Experimental investigation of cement hydration in gravity-free environment

Juliana Neves, Richard Grugel, Barry Scheetz, and Aleksandra Radlinska

ABSTRACT

In this work, cement hydration in terrestrial and microgravity environment was compared. This was for the first time, when the International Space Station was utilized to fully investigate the complex process of cement solidification. Microstructural development of hydrating cement occurs in stages during the hydration reaction and hardening process, which results in elaborate combinations of amorphous and crystalline phases. The morphology, volume fraction, and distribution of these phases ultimately determine the hardened cement's material properties. Minimizing gravity-driven phenomena, such as thermosolutal convective flow and sedimentation ensures crystal growth strictly by diffusion and a microstructure forms differently from that observed in typical laboratory conditions on Earth.

A test matrix was developed that includes samples with various w/c ratio and various compositions; incorporating alite, pure water and cement system, cement with chemical admixtures, as well as commercial products. This paper reports on main changes initially observed in the microstructural development of hydrated pure compound of tricalcium silicate (C3S).

1. INTRODUCTION

This paper reports on initial findings of the Microgravity Investigation of Cement Solidification (MICS) research project that was conducted in the microgravity environment aboard the International Space Station (ISS). The experiments consisted of mixing and hydrating cement in the gravity-free environment. Minimizing gravity-driven transport phenomena, such as buoyancy, convection, and sedimentation ensures solidification through slower, chemical-driven, diffusion; a factor considerably different from that of typical laboratory conditions on Earth. Consequently, different microstructures and, consequently, altered material properties are expected between 1g and μg hydrated cement. Understanding these results can have implications to future processing of cement-based materials on Earth, as well as infrastructure development on extraterrestrial bodies.

This work describes the main changes initially observed in the microstructural development of tricalcium silicate (C_3S) samples that were hydrated aboard the ISS. Since C_3S makes up about 50 percent of typical portland cements and dictates most of the early reaction kinetics and paste characteristics (Mindess, Young, & Darwin, 2003; Scrivener, 2004; Taylor, 1990), it was selected as primary material of interest. Analysis of the single component system should also, in principle, provide a guide for later investigation of more complexes systems, such as portland cement mixtures.

2. MATERIALS AND METHODS

2.1 Characterization of tricalcium silicate (C_3S)

High purity triclinic C_3S powder (3500 cm^2/gram surface area) was obtained from Mineral Research Processing (Meyzieu, France). Dry-dispersion laser diffraction (Malvern Mastersizer 3000) was conducted to determine the particle size distribution. Approximately 100 mg of powder was dispersed by an Aero S dry dispersion unit using a standard venturi at 4 bar air pressure and a 25% feed rate. The refractive index and adsorption were assumed per Malvern software, to be, respectively, 1.68 and 0.1. Table 1 shows D10, D50, and D90 (□m) at which 10%, 50% and 90% of the particles, respectively, are smaller than the indicated value. For example, assuming the particles have a spherical shape, 10% of the analyzed particles have a diameter equal to or smaller than 1.60 □m.

Table 1. Percentage of C_3S particles with a diameter equal to or smaller than the indicated values

	D10	D50	D90
Average diameter (μm)	1.60	5.22	12.88
Standard Dev.	0.14	0.16	0.77

2.2 Mixture proportioning

Pure C_3S and lime-water were mixed at a water-to-cement ratio (w/c) of 2.0, by mass. The large amount of water per C_3S was chosen to ensure complete hydration of the powder and to increase the porosity, which allows unobstructed growth of the portlandite crystals. Each sample consisted of 5 grams of C_3S and 10 grams of lime-water. The lime-water consisted of a supersaturated solution (15mmol/liter) of calcium hydroxide where 1.12 grams of calcium hydroxide was added to 1000 grams (1 liter) of deionized water, then sealed, and subsequently continuously stirred for 24 hours at room temperature to ensure stabilization of the solution. The paste mixture was prepared by combining C_3S with lime-water rather than pure water in order to control the initial reaction rate, given the high w/c ratio (Hu, Aboustait, Kim, Ley, Bullard, et al., 2016; Hu, Aboustait, Kim, Ley, Hanan, et al., 2016).

2.3 Experimental Setup

Commercially available plastic containers (Burst Pouches®) having an internal burstable seal were used to combine the mixture ingredients. The pouches were prepared on Earth by filling the respective pouch compartments with anhydrous cementitious materials (i.e. C_3S) and aqueous solutions (i.e. lime water). For each sample pouch sent to the ISS on the OA9 resupply mission, an identical one was prepared as a ground-control. The space and ground samples were mixed simultaneously and stored at the same temperature conditions (20 ºC □ 2 ºC). The pressure and relative humidity conditions (1 ATM and 35%

RH) are characteristics of the air trapped within the pouches, and as such were also constant between ground and space samples. Thus gravity, or lack of, is considered the only variable between space and ground samples.

Figure 1 illustrates how the astronauts processed the samples within a glovebag aboard the ISS. The mixing procedure consisted of exerting pressure on the liquid phase by tightly rolling the pouch from one end until the internal seal ruptured, which allowed the water to contact the anhydrous powder. Then hydrating cement paste was then manually mixed, primarily with a rubberized spatula for approximately 3 minutes, or until homogeneity was achieved. Finally, a clamp was used to assure consolidation of the paste. The processed pouches were maintained undisturbed and allowed to hydrate for six weeks aboard the ISS until return to Earth for analysis. It is worth noting that the mixture remained within the sealed pouch for the entire duration of the experiment, until analysis on Earth. Typical processed sample (with clamp removed already) has been shown in Figure 2.

Figure 1. Astronaut Alex Gerst processing a MICS sample aboard the ISS (photo credit: NASA)

Figure 2. A typical processed pouch with a hydrating paste

2.4 Scanning electron microscopy (SEM)

A few days after their return to Earth, the hardened samples were removed from the pouches inside an argon filled glovebox, and then fractured by cleaving through the mid-section. After the sample was prepared for examination, it was immediately placed in a Hitachi S-3700N scanning electron microscope (SEM) so that the fracture surface could be examined. Sample examination was conducted under variable pressure conditions (10 to 20 Pa) with an acceleration voltage of 10 or 15 keV. A probe current of 25 □A and an aperture of 4 were used to maximize image resolution of the backscattered (BSE) micrographs.

In addition, images of polished surface were taken to better visualize the microstructure of the portlandite crystals. Here, sample preparation consisted of removing the hardened paste from the pouch and soaking it in 200 ml of isopropanol alcohol for 48 hours and then dried in vacuum for 30 hours. Subsequently, the samples were mounted in epoxy, ground through a series of SiC paper, final polished with 0.25 μm diamond paste and carbon coated. An FEI Q250 SEM was used for imaging, and the specific conditions are shown at each image.

2.5 Mercury intrusion porosimetry (MIP)

The sample preparation for MIP consisted of immersing ground and space samples individually in 200 ml of isopropyl alcohol for 48 hours for solvent exchange. The samples then underwent 34 hours of drying under vacuum at room temperature. Subsequently, a Micromeritics AutoPore V 9620 MIP mercury penetrometer was used to assess the porosity, pore size distribution, bulk density, and skeletal density of the pastes. The mercury temperature during testing of ground and space samples was 19 ºC.

3. RESULTS AND DISCUSSION

3.1 SEM

SEM images of the ground (control) and space cement pastes show a number of differences. To begin, the μ*g* sample, Figure 3, shows a significantly greater amount of trapped air, as evidenced by the large, round shell-like structures. This can be expected given the lack of buoyancy in the space-processed samples. Buoyancy is a gravity-driven phenomenon that results from differences of specific gravities in the components comprising a given system (Turner, 1979). Under the influence of gravity, air bubbles, for example, are expected to move upwards through the initial watery cement paste due to their lower density (1.2 kg/m^3 (Cavcar, 2000)) while also promoting fluid flow (Barge et al., 2015).

Furthermore, Figure 3 suggests that the C_3S hydrated in microgravity has higher porosity and/or bigger pores in comparison to the ground control, which could also be expected in absence of gravity-driven settlement. This hypothesis was further examined and the MIP section of this manuscript addresses the differences found.

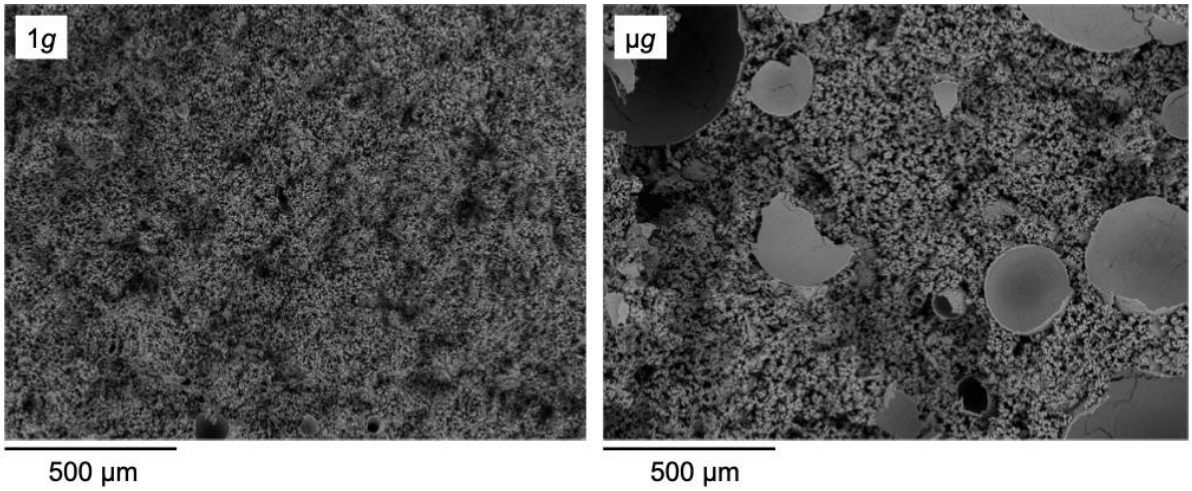

Figure 3. Fractured cross section of 54 days-old C_3S paste hydrated in 1g and g

Polished SEM images of ground and space samples are shown in Figure 4 and Figure 5, respectively. The overall microstructure contrasts significantly between the two images, particularly regarding porosity and the portlandite morphology. It can be seen that the CH crystals are smaller and more prismatic when grown under gravity conditions, whereas larger and more plate-like when grown under microgravity conditions. (Fontana, Schefer, & Pettit, 2011) reported an atypical morphology of sodium chloride (NaCl) when the crystals grew aboard the ISS, under microgravity conditions. Differences in ettringite morphology due to changes in gravity level has been previously reported by Plank and co- workers (Lei et al., 2016; Meier & Plank, 2016; Meier, Sarigaphuti, Sainamthip, & Plank, 2015). However, the studies were conducted aboard a parabolic flight that provides only 10 seconds of μ*g*, and the findings are limited to instantaneous or "flash" ettringite formation.

For a clearer understanding of the differences observed between samples hydrated in 1*g* and μ*g*, it is essential to look closely at the typical gravity-driven effects on the hydration of cementitious pastes. Figure 6 shows sedimentation layers formed in the 3 milimiter-thick ground control sample. The yellow arrow represents the direction of the gravity, along with the direction of a porosity gradient. This happens early in the hydration due to sinking of anhydrous C_3S particles (specific gravity of 3.15) and raise of the calcium-saturated water. It results in a gradient water-to-cement ratio, which is higher on the top and lower on the bottom of the samples, leading to, respectively, higher porosity and lower porosity. Additionally, the excess calium-saturated water on the top allows large portlandite (CH) crystals to grow at the surface, which is also shown in Figure 6. This phenomenon is commonly referred as the bleeding effect.

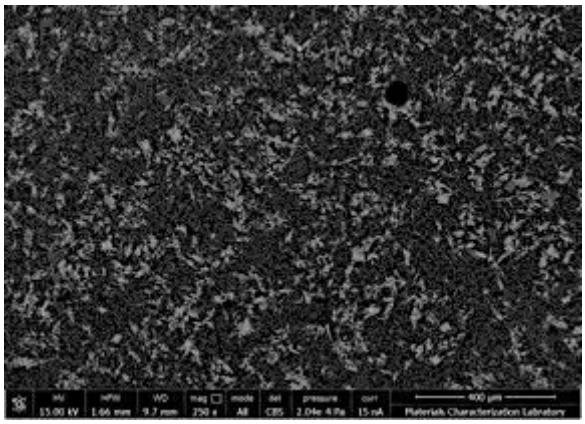

Figure 4: **Polished surface of C_3S sample hydrated in 1*g* condition (control). The light grey corresponds to the portlandite crystals, the intermediate grey to C-S-H cluster, and the dark grey to porosity. The dark grey can be barely seen in this image due to the low porosity of the sample.**

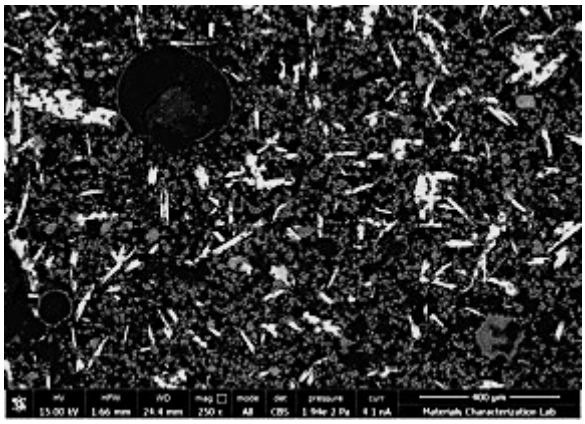

Figure 5: Polished surface of C_3S hydrated in µ*g* condition. The light grey corresponds to the portlandite crystals, the intermediate grey to C-S-H cluster, and the dark grey to porosity and air voids. A much higher porosity can be noted comparing to Figure 4.

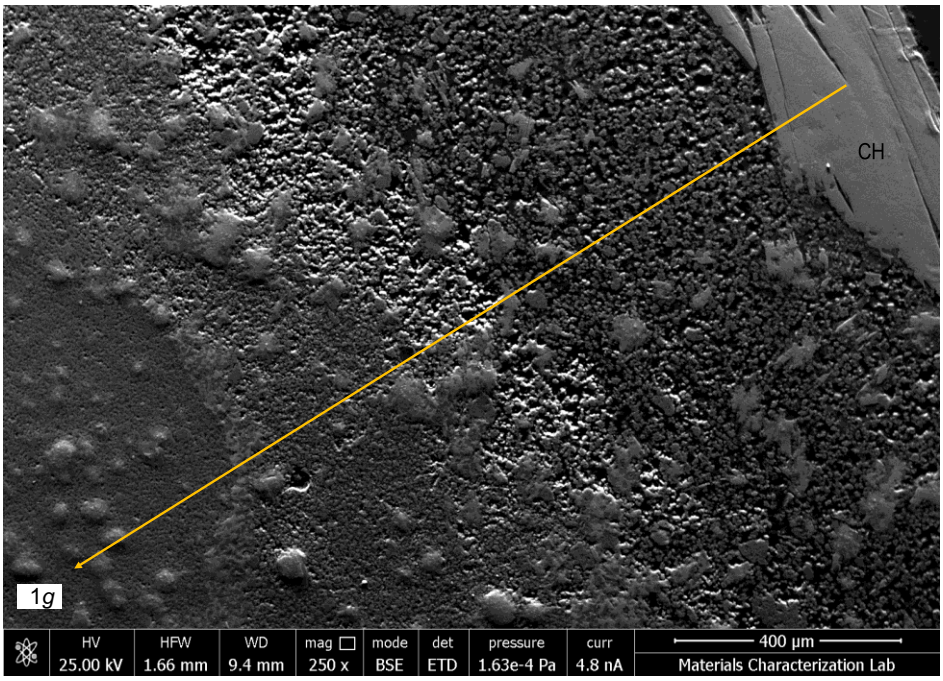

Figure 6. Sedimentation layers of C_3S paste hydrated in 1*g* environment (polished sample)

Given the existence of a porosity gradient, it is worthy comparing both top and bottom of the 1*g* specimen to the uniform µ*g* matrix. Figure 7 shows the top of the polished cross section of the 1*g* sample, while Figure 8 shows the cross section of the µ*g* sample. By comparison, the µ*g* sample still seems to be more porous and have larger pores than the top section of the 1*g* sample. Once again, the portlandite greatly differs between ground and space samples. It can be noticed that the portlandite formed in 1*g* grows in the direction of the basal plane (i.e. “c” direction), whereas that formed in µ*g* grows in the direction of the lateral facets (i.e., “a” direction), providing the crystals with different aspect ratios. The a-to-c ratio (a/c) is smaller than 1 when formed under 1*g* (Figure 7), and it is much higher than 1 when hydrated in µ*g* (Figure 8). Even though the top of 1*g* samples are highly porous, the great majority of the portlandite crystals have a/c smaller than one, which suggests that a parameter other than porosity also affects the CH growth orientation. As shown by (Harutyunyan, Kirchheim, Monteiro, Aivazyan, &

Fischer, 2009), a typical, preferred aspect ratio of portlandite is 2.7 or larger, which is in agreement with the crystals formed in μ*g*.

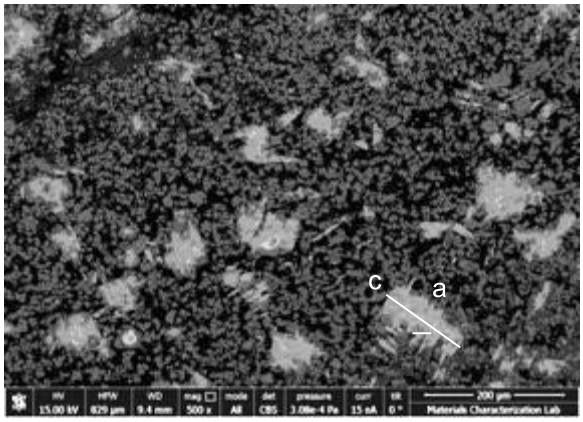

Figure 7: Top of the polished surface of C_3S hydrated in 1*g* condition. The darkest gray represents porosity, and the lightest grey are portlandite crystals or clusters. The basal (c) direction and lateral (a) directions are showing a/c < 1

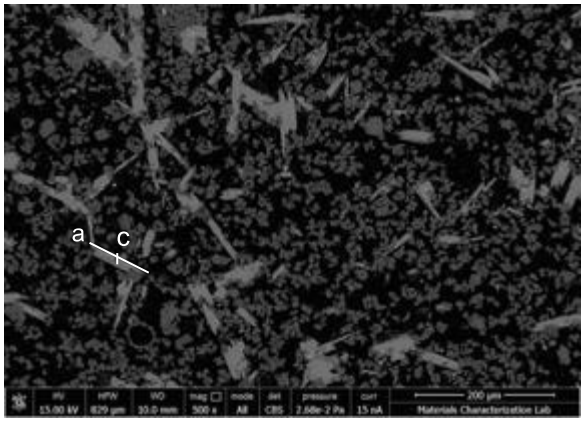

Figure 8: Polished surface of C_3S hydrated in μ*g* condition, showing higher porosity than the top of 1*g* sample. The darkest gray represents porosity, and the lightest grey are portlandite crystals or clusters. The basal (c) direction and lateral (a) directions are showing a/c >> 1

Figure 9 shows the bottom of the polished cross section of the 1*g* sample, while Figure 10 presents the cross section of the μ*g* sample. The porosity (darker gray) in the ground sample can barely be noticed in Figure 9; the portlandite seems to grow intermixed with the C-S-H (intermediate gray) and show indefinite morphology, as shown by Gallucci and coworkers (Gallucci & Scrivener, 2007). Figure 10, conversely, shows a highly porous matrix and well defined portlandite crystals/clusters of high aspect ratio (a/c >>1), as discussed prior. Figures 11 and 12 show the fractured surfaces of ground and space samples and how the crystals morphologies are displayed among the C-S-H matrix.

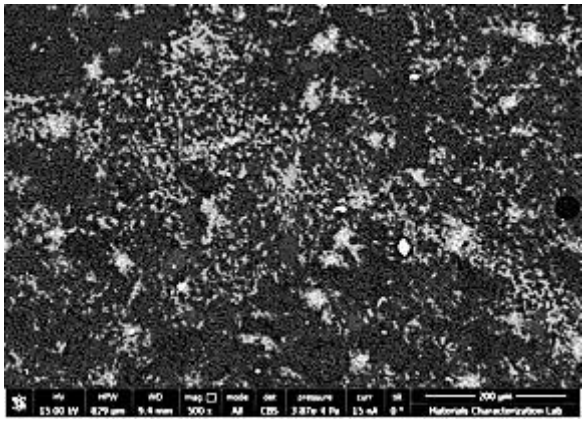

Figure 9: Bottom of the polished surface of C_3S hydrated in 1*g* condition, showing very low porosity and portlandite grown intermixed with the C-S-H phase

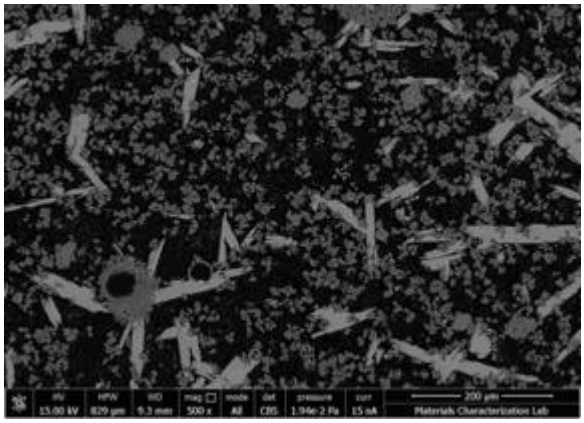

Figure 10: Polished surface of C_3S hydrated in μ*g* condition; portlandite crystals showing well defined morphology and a/c >> 1

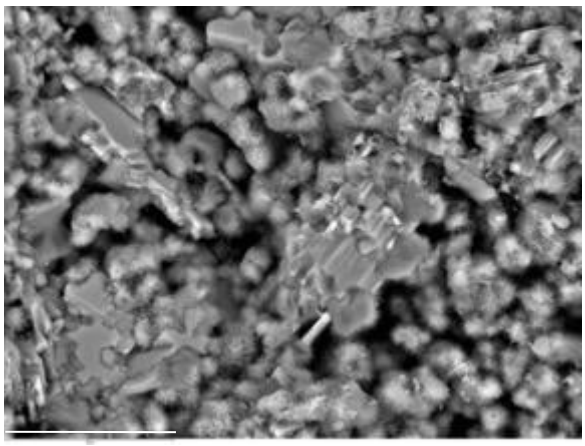

Figure 11: Bottom of the fractured surface of C_3S hydrated in 1*g* condition, showing low aspect ratio portlandite intermixed with the C-S-H phase. Scale bar of 25 µm

Figure 12: Fractured surface of C_3S hydrated in µ*g* condition, showing high aspect ratio portlandite with well defined morphology. Scale bar of 25 µm

The changes seen in portlandite morphology formed under µg are then attributed to (1) bigger pores and higher porosity, which provide the crystals with extra room for growth, and (2) absence of convection, buoyancy, and sedimentation, which limits mass transport through fluid flow. Lacking the gravity-driven fluid flow results in a purely diffusion-controlled mass transport and, likely, in an extended induction period and slower rate of hydration. A slower hydration enables the calcium species to attach to an existing crystal, which is known to be preferential over forming nuclei (Gallucci & Scrivener, 2007), and sustain its preferential growth orientation (Harutyunyan et al., 2009).

3.2 MIP

The MIP-measured porosity of ground and space samples were 48.4 and 69.4 percent, respectively, in line with the visual SEM observations. Lamentably, it is not possible to distinguish between the porosity from the top and bottom of the ground sample, and the value of 48.4 is reported as the average. It worth noting that the porosity was expected to be high due to w/c of 2.0 for both ground and space pastes.

Figure 13 shows the pore size distribution of the pastes hydrated in 1*g* and µ*g*, which is also in agreement with the SEM micrographs. As it can be observed, the paste hydrated in 1g develops well-distributed pore sizes, whereas the paste hydrated in µg shows 50 percent of the pores larger than 6,015 nm. This can be seen graphically by the steep slope within the range of 6,000-10,000 nm. It is well known that the porosity and pore size distribution strongly affects mass transport (Bentz & Garboczi, 1991; Kim et al., 2012), conductivity (Rajabipour & Weiss, 2007), and mechanical properties (Powers, 1958; Young & Hansen, 1987) of cement-based system.

Additionally, as shown in Figure 13, about 7 percent of the pores in the µ*g* sample falls under the 10 nm-range, which is considered to be gel porosity, an intrinsic part of the C-H-S. It is possible that this is an artefact due to limitations of the technique, at which the mercury is impeded to access smaller pores (Aligizan, 2006). Despite this, it is possible that the gel porosity also differs between 1*g* and µ*g* hydration environments.

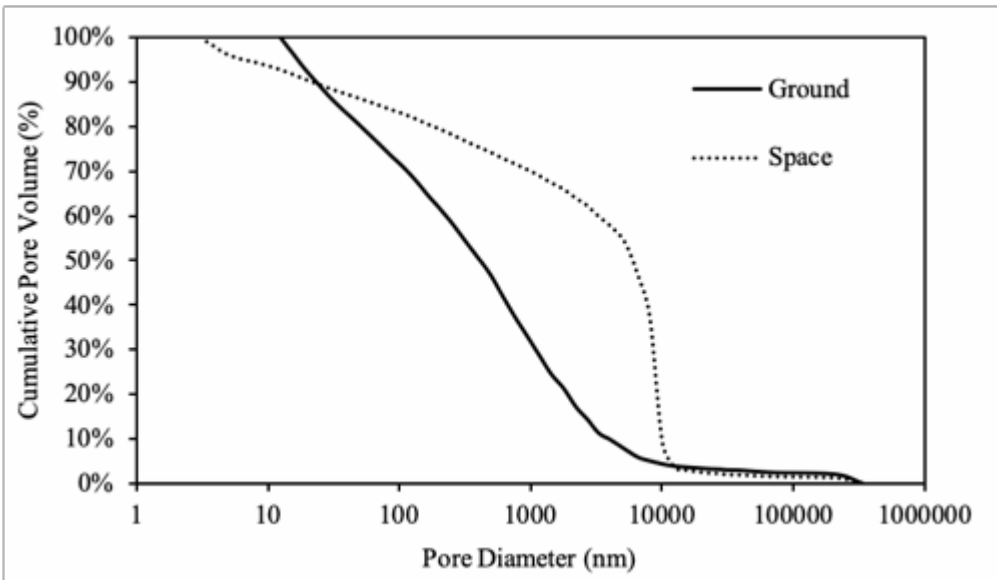

Figure 13. Pore size distribution of C_3S pastes hydrated in 1*g* and µ*g* environment

4. CONCLUSIONS

Initial results (SEM micrographs and x-ray diffraction scans) show distinct differences between the microstructure of C_3S hydrated in 1*g* and µ*g*. To date, the most pronounced changes seen in C_3S hydrated in µg are an increase in porosity and larger pore diameters due to lack of sedimentation. Morphological differences in the calcium hydroxide (CH) crystals grown in µ*g* are also observed. In microgravity, CH develops a plate-like morphology and seem less frequently distributed in comparison to the ground sample, which is attributed primarily to the slower hydration rate. The slower hydration allows the portlandite growth to be purely chemically-driven enhancing its preferred orientation.

5. ACKNOWLEDGEMENTS

The authors gratefully acknowledge the financial support from the National Aeronautics and Space Administration (NASA) - Grant No. NNX17AC48G, as well as the use of MSFC's EM31 Materials Diagnostics laboratory. The assistance of Dale Bentz and Jeff Bullard from NIST in this research is gratefully acknowledged.

6. REFERENCES

Aligizan, K. K. (2006). *Pore structure of cement-based materials - testing, interpretation and requirements*. (A. Bentur & S. Mindess, Eds.). New York, Abingdon [England]: Taylor & Francis.

Barge, L. M., Cardoso, S. S. S., Cartwright, J. H. E., Cooper, G. J. T., Cronin, L., De Wit, A., … Thomas, N. L. (2015). From chemical gardens to chemobrionics. *Chemical Reviews*, *115*(16), 8652–8703. https://doi.org/10.1021/acs.chemrev.5b00014

Bentz, D. P., & Garboczi, E. J. (1991). Percolation of phases in a three-dimensional cement paste microstructural model. *Cement and Concrete Research*, *21*, 325–344.

Cavcar, M. (2000). *The International Standard Atmosphere*.

Fontana, P., Schefer, J., & Pettit, D. (2011). Characterization of sodium chloride crystals grown in microgravity. *Journal of Crystal Growth*, *324*(1), 207–211. https://doi.org/10.1016/j.jcrysgro.2011.04.001

Gallucci, E., & Scrivener, K. (2007). Crystallisation of calcium hydroxide in early age model and ordinary cementitious systems. *Cement and Concrete Research*, *37*(4), 492–501.

https://doi.org/10.1016/j.cemconres.2007.01.001

Harutyunyan, V. S., Kirchheim, A. P., Monteiro, P. J. M., Aivazyan, A. P., & Fischer, P. (2009). Investigation of early growth of calcium hydroxide crystals in cement solution by soft X-ray transmission microscopy. *Journal of Materials Science*, *44*(4), 962–969. https://doi.org/10.1007/s10853-008-3198-5

Hu, Q., Aboustait, M., Kim, T., Ley, M. T., Bullard, J. W., Scherer, G., … Gelb, J. (2016). Direct measurements of 3d structure, chemistry and mass density during the induction period of C3S hydration. *Cement and Concrete Research*, *89*, 14–26. https://doi.org/10.1016/j.cemconres.2016.07.008

Hu, Q., Aboustait, M., Kim, T., Ley, M. T., Hanan, J. C., Bullard, J., … Rose, V. (2016). Direct three-dimensional observation of the microstructure and chemistry of C3S hydration. *Cement and Concrete Research*, *88*, 157–169. https://doi.org/10.1016/j.cemconres.2016.07.006

Kim, K. Y., Yun, T. S., Park, K. P., Mo, L., Panesar, D. K., Hu, J., … Dangla, P. (2012). Pore structure characterization of cement pastes blended with high-volume fly-ash. *Cement and Concrete Research*, *42*(6), 769–777. https://doi.org/10.1016/j.cemconres.2013.03.020

Lei, L., Meier, M. R., Rinkenburger, A., Zheng, B., Fu, L., & Plank, J. (2016). Early Hydration of Portland Cement Admixed with Polycarboxylates Studied Under Terrestric and Microgravity Conditions. *Journal of Advanced Concrete Technology*, *14*(3), 102–107. https://doi.org/10.3151/jact.14.102

Meier, M. R., & Plank, J. (2016). Crystal growth of [Ca3Al(OH)6.12H2O]2.(SO4)3.2H2O (ettringite) under microgravity: On the impact of anionicity of polycarboxylate comb polymers. *Journal of Crystal Growth*, *446*, 92–102. https://doi.org/10.1016/j.jcrysgro.2016.04.049

Meier, M. R., Sarigaphuti, M., Sainamthip, P., & Plank, J. (2015). Early hydration of Portland cement studied under microgravity conditions. *Construction and Building Materials*, *93*, 877–883. https://doi.org/10.1016/j.conbuildmat.2015.05.074

Mindess, S., Young, J. F., & Darwin, D. (2003). *Concrete* (Second Edi). Pearson Education, Inc.

Powers, T. C. (1958). Structure and physical properties of hardened Portland cement paste. *Journal of the American Ceramic Society*, *41*(1), 1–6.

Rajabipour, F., & Weiss, J. (2007). Electrical conductivity of drying cement paste. *Materials and Structures*, *40*(10), 1143–1160. https://doi.org/10.1617/s11527-006-9211-z

Scrivener, K. L. (2004). Backscattered electron imaging of cementitious microstructures: understanding and quantification. *Cement and Concrete Composites*, *26*, 935–945. https://doi.org/10.1016/j.cemconcomp.2004.02.029

Taylor, H. F. W. (1990). *Cement Chemistry*. New York: Academic Press.

Turner, J. S. (1979). *Buoyancy effects in fluids*. Cambridge University Press.

Young, J. F., & Hansen, W. (1987). Volume relationships for C-S-H formation based on hydration stoichiometries. *Materials Research Society*, *85*, 313–322.